

Comparison of optimal actuation patterns for flagellar magnetic micro-swimmers

Yacine E. Faris ^{*,**} Jean-Baptiste Pomet ^{*} Stéphane Régnier ^{**}
Laetitia Giraldi ^{*}

^{*} *Université Côte d'Azur, Inria, CNRS, LJAD, McTAO team, Nice,
France.*

^{**} *Sorbonne Université, CNRS, ISIR, Paris, France*

Abstract: In this article, we present a simplified model of a flagellar micro-swimmer actuated by external magnetic fields that is based on shape discretization and an approximation of the hydrodynamical forces. We numerically solve the optimal control problem of finding the actuating magnetic fields that maximizes its horizontal propulsion speed over a fixed time under different constraints on the magnetic field amplitudes and compare the optimal solutions. All the simulated magnetic fields out-perform the standard sinusoidal actuation method that is prevalent in the literature and in experiments. Moreover, non-planar constraints on the control leads to novel optimal trajectories for flagellar low-Reynolds swimmers and perform significantly better than planar actuation.

Keywords: Optimal control, Low-Reynolds Swimmers, Magnetic micro-swimmers, Soft Robotics

1. INTRODUCTION

Robotic micro-swimmers have the potential to conduct small-scale operations such as targeted drug delivery (Qiu et al. (2015); Patra et al. (2013)), and minimally invasive medical diagnosis and surgery (Mack (2001); Fusco et al. (2014)). The design and way of locomotion of these devices is based on biological swimming micro-organisms, and wireless actuation methods are often chosen over built-in energy sources because of the difficulties of miniaturizing the latter. In particular, the actuation of partially magnetized micro-swimmers via external time-varying magnetic fields has proven to be an effective way to induce propulsion at the micro-scale (Dreyfus et al. (2005); Ye et al. (2014); Qiu et al. (2015)).

In this paper, we focus on flexible magnetic micro-swimmers that are based on flagellar cells in their design. By magnetizing the tail (Dreyfus et al. (2005)) or the head (Khalil et al. (2014); Oulmas et al. (2017)) of the swimmer, the propulsion of the swimmer in a straight line is obtained in experimental settings by applying the superposition of a static magnetic field to orient the swimmer in the desired direction and an oscillating magnetic field perpendicular to the swimmer, which leads to a planar beat of its tail. Dynamic models of flexible microswimmers (whether robotic or biological) are often based on hydrodynamics and continuum mechanics (elasticity), and expressed with partial differential equations that are numerically expensive and thus often reduced to the planar case (Lowe (2003); Tornberg and Shelley (2004)). This complexity makes such models ill suited for the numerical resolution of optimal control problems related to the actuation of flexible micro-swimming robots such as minimal-cost trajectory planning.

We present a simple and numerically cheap dynamical

model of a flagellar micro-swimmer in 3D and use it to investigate optimal magnetic actuation patterns for horizontal propulsion. After discretizing the shape of the tail of the swimmer, we use Resistive Force Theory (Gray and Hancock (1955)) to approximate the hydrodynamics of the system, generalizing the planar 'N-link Swimmer' models from Moreau et al. (2018) and Alouges et al. (2013, 2015). We numerically solve the optimal control problem of finding the actuating magnetic field that maximizes the horizontal displacement of the swimmer during a fixed time. We investigate four different types of constraints on the control: firstly, we consider the feasible controls to be the superposition of static orientating field along the prescribed swimming direction and a time-varying orthogonal actuating field, which leads to a single-input optimal control problem. Secondly, we consider the control to be a two-dimensional magnetic field where both components are time-varying. Lastly, we consider two three-dimensional magnetic fields that leads to out-of-plane optimal trajectories: one with a static orientating component and two orthogonal time-varying fields, and one where all three components are time-varying.

One of the main conclusions that stems from the numerical solutions of these optimal control problems is the periodicity of the optimal magnetic fields in the all cases (modulo edge effects) and the periodicity of the deformation undergone by the tail of the swimmer when actuated by these magnetic fields. Furthermore, we show that all the solutions out-perform by large the standard sinusoidal fields used in experiments, especially the non-planar solutions. Another result shown by the simulations is that static orientating magnetic fields are not necessary for horizontal propulsion, and that propulsion speed is significantly improved where all the magnetic field components are free to be optimized.

This paper is organized as follows : first, we describe our swimmer model and derive its dynamics then, we formulate the maximum-displacement optimal control problems, assuming that we want the micro-robot to swim in the x -direction and present the numerical solutions of the problems. Lastly, we discuss influence of the number of links of the tail of the swimmer on the solutions of the optimal control problems.

2. 3D FLAGELLAR MAGNETIC MICRO-SWIMMER MODEL

The micro-swimmer model used in this study is a 3D generalization of the planar swimmer models of Moreau et al. (2018) and Alouges et al. (2013, 2015). We consider a swimmer of the form of a magnetized spherical head attached to an articulated chain of N slender rods of length l that can rotate with respect to each other with elastic torques that tend to keep them aligned. We assume that the swimmer is immersed in an unbounded domain of a viscous fluid and that it swims at a low Reynolds number. Under these assumptions, we neglect the inertial effects on the swimmer in favor of the viscous effects and use the Resistive Force Theory (RFT) framework (Gray and Hancock (1955)) to simplify the fluid-structure interaction.

2.1 Kinematics of the swimmer

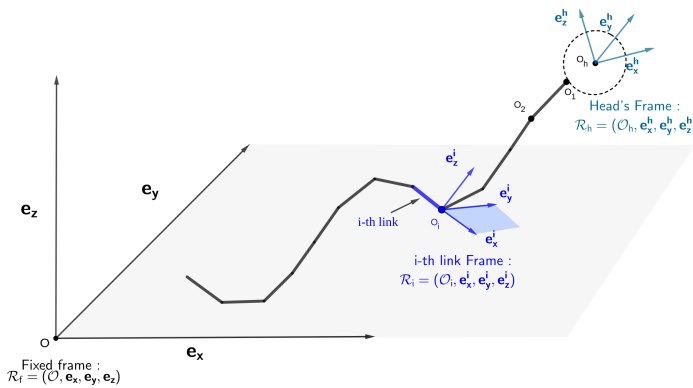


Fig. 1. Reference and local frames of the discrete-shape model. The swimmer's head frame is oriented relative to the reference frame. For each link i , the corresponding local frame \mathcal{R}_i is oriented relative to \mathcal{R}_h .

We associate to the head of the swimmer the moving frame $\mathcal{R}_{head} = (O_h, \mathbf{e}_x^h, \mathbf{e}_y^h, \mathbf{e}_z^h)$, where O_h is the center of the head. The orientation of each link i is represented by the moving frame $\mathcal{R}_i = (O_i, \mathbf{e}_x^i, \mathbf{e}_y^i, \mathbf{e}_z^i)$, where O_i is the extremity of the i -th link. We define $R_{head} \in SO(3)$ as the rotation matrix that allows the transformation of coordinates from the fixed reference frame to \mathcal{R}_{head} and the matrices $R_i \in SO(3)$, for $i = 1 \dots N$, as the relative rotation matrix that transforms coordinates from \mathcal{R}_{head} to \mathcal{R}_i . R_{head} is parametrized by a $(X - Y - Z)$ rotation sequence $(\theta_x, \theta_y, \theta_z)$ and each relative rotation matrix R_i is parametrized by a $Y - Z$ rotation sequence : (ϕ_y^i, ϕ_z^i) relative to the head's frame. Using these notations, the swimmer is represented by two sets of variables : The *Position variables*: (\mathbf{X}, Θ) where

$$\begin{aligned} \mathbf{X} &= (x_h, y_h, z_h) \in \mathbb{R}^3 \text{ and} \\ \Theta &= (\theta_x, \theta_y, \theta_z) \in [0, 2\pi]^3, \end{aligned} \quad (1)$$

and the $2N$ *Shape variables*, denoted by

$$\Phi = (\phi_y^1, \phi_z^1, \dots, \phi_y^N, \phi_z^N) \in [0, 2\pi]^{2N}. \quad (2)$$

2.2 Dynamics of the swimmer

The RFT framework neglects the global interactions between the swimmer and the surrounding fluid in favor of the local anisotropic friction of the slender body with the surrounding fluid. This results in explicit expressions of the density of force applied by the fluid to the swimmer that are linear with respect to $(\dot{\mathbf{X}}, \dot{\Theta}, \dot{\Phi})$. More precisely, We consider a hydrodynamical drag force \mathbf{F}_{head}^h acting on the head of the swimmer that is proportional to its velocity in each of the direction of the head's frame's vectors \mathcal{R}_{head} and a hydrodynamical torque on the head that is proportional to its angular velocity :

$$\begin{aligned} \mathbf{F}_{head}^h &= -R_{head} D_H R_{head}^T \dot{\mathbf{X}} \\ \mathbf{T}_{head}^h &= -k_R \Omega_{head}. \end{aligned} \quad (3)$$

where $k_{H,\parallel}$, $k_{H,\perp}^1$, and $k_{H,\perp}^2$ are positive real numbers that represents the hydrodynamic drag coefficients of the head along the $\mathbf{e}_x^h, \mathbf{e}_y^h$ and \mathbf{e}_z^h direction, D_H is the matrix $\begin{pmatrix} k_{H,\parallel} & 0 & 0 \\ 0 & k_{H,\perp}^1 & 0 \\ 0 & 0 & k_{H,\perp}^2 \end{pmatrix}$, k_R is the rotational drag coefficient of the head and Ω_{head} is the angular velocity vector of the head of the swimmer.

To compute the hydrodynamic effects on each link $i \in (1, \dots, N)$ of the tail, we consider the hydrodynamic force density $\mathbf{f}_i(s)$ acting on a point $\mathbf{x}_i(s)$ parametrized by its arclength s . Following Resistive Force Theory, the expression of $\mathbf{f}_i(s)$ reads :

$$\begin{aligned} \mathbf{f}_i(s) &= -k_{\parallel} (\mathbf{V}_i(s) \cdot \mathbf{e}_x^i) \mathbf{e}_x^i - k_{\perp} (\mathbf{V}_i(s) \cdot \mathbf{e}_y^i) \mathbf{e}_y^i \\ &\quad - k_{\perp} (\mathbf{V}_i(s) \cdot \mathbf{e}_z^i) \mathbf{e}_z^i \end{aligned} \quad (4)$$

where k_{\parallel} and k_{\perp} are respectively the parallel and perpendicular drag coefficients of the swimmer and $\mathbf{V}_i(s)$ is the velocity of $\mathbf{x}_i(s)$.

The drag force on link i , \mathbf{F}_i^h , and hydrodynamic torques on each link i (about the extremity O_j of link j derive from the force densities as follows:

$$\mathbf{F}_i^h = \int_0^l \mathbf{f}_i(s) ds, \quad (5)$$

and

$$\forall j \in (1 \dots N) \quad \mathbf{T}_{i,O_j}^h = \int_0^l (\mathbf{x}_i(s) - \mathbf{O}_j) \times \mathbf{f}_i(s) ds, \quad (6)$$

where l is the length of each link.

We consider that the head of the swimmer is magnetized along the \mathbf{e}_x^h axis. Denoting by \mathbf{M} the magnetization vector of the head and considering an external homogeneous time-varying field $\mathbf{B}(t)$, the following torque is applied to the swimmer

$$\mathbf{T}^{mag} = \mathbf{M} \times \mathbf{B}(t). \quad (7)$$

The acceleration terms in the dynamics are neglected due to the Low Reynolds assumption (Yates (1986)), thus, the balance of forces and torques applied on the swimmer gives:

$$\left\{ \begin{array}{l} \mathbf{F}_{head}^h + \sum_{i=1}^N \mathbf{F}_i^h = \mathbf{0}_3, \\ \mathbf{T}_{head}^h + \sum_{i=1}^N \mathbf{T}_{i,H}^h = -\mathbf{T}^{mag}, \end{array} \right. \quad (8)$$

which leads to 6 independent equations. In addition to these equations, we take the internal contributions of the tail and its elasticity into account by adding the balance of torque on each subsystem consisting of the chain formed by the links i to N for $i = 1 \dots N$. These $3N$ equations reduce to $2N$ non-trivial equations by taking only the components perpendicular to the link k when calculating the sum of the torques from k to N . The elasticity of the tail is discretized by considering a restoring elastic moment \mathbf{T}_i^{el} at each joint O_i that tends to align each pair $(i, i + 1)$ of adjacent links with each other:

$$\mathbf{T}_i^{el} = k_{el} \mathbf{e}_x^i \times \mathbf{e}_x^{i-1}. \quad (9)$$

Thus, the dynamics of the swimmer are described the following system of $2N + 6$ equations :

$$\left\{ \begin{array}{l} \mathbf{F}_{head}^h + \sum_{i=1}^N \mathbf{F}_i^h = \mathbf{O}_3, \\ \mathbf{T}_{head}^h + \sum_{i=1}^N \mathbf{T}_{i,H}^h = -\mathbf{T}^{mag}, \\ \sum_{i=1}^N \mathbf{T}_{i,1}^h \cdot \mathbf{e}_y^1 = -\mathbf{T}_1^{el} \cdot \mathbf{e}_y^1, \\ \sum_{i=1}^N \mathbf{T}_{i,1}^h \cdot \mathbf{e}_z^1 = -\mathbf{T}_1^{el} \cdot \mathbf{e}_z^1, \\ \vdots \\ \vdots \\ \mathbf{T}_{N,N}^h \cdot \mathbf{e}_y^n = -\mathbf{T}_n^{el} \cdot \mathbf{e}_y^n, \\ \mathbf{T}_{N,N}^h \cdot \mathbf{e}_z^n = -\mathbf{T}_n^{el} \cdot \mathbf{e}_z^n. \end{array} \right. \quad (10)$$

Following Resistive Force Theory, and the definition of the drag densities, the hydrodynamic contributions (left-hand side of the previous system) are linear with respect to the angular and translational velocities, thus, the previous equation can be rewritten matricially in the form :

$$M^h(\Theta, \Phi) \begin{pmatrix} \dot{\mathbf{X}} \\ \dot{\Theta} \\ \dot{\Phi} \end{pmatrix} = B(\mathbf{X}, \Theta, \Phi). \quad (11)$$

, where $M^h(\Theta, \Phi) \in \mathbb{R}^{(2N+6) \times (2N+6)}$ represents the hydrodynamical effects on the swimmer and the right-hand side $B(\mathbf{X}, \Theta, \Phi) \in \mathbb{R}^{2N+6}$ corresponds to the magnetic and elastic contributions on the swimmer.

The previous equation can be rewritten as a control system, where the dynamics of the swimmer are affine with respect to the components of the actuating magnetic field viewed as a control:

$$\begin{pmatrix} \dot{\mathbf{X}} \\ \dot{\Theta} \\ \dot{\Phi} \end{pmatrix} = \mathbf{F}_0(\Theta, \Phi) + (\mathbf{B}_x(t) \ \mathbf{B}_y(t) \ \mathbf{B}_z(t)) \begin{pmatrix} \mathbf{F}_1(\Theta, \Phi) \\ \mathbf{F}_2(\Theta, \Phi) \\ \mathbf{F}_3(\Theta, \Phi) \end{pmatrix} \quad (12)$$

where the vector fields F_0, \dots, F_3 are functions of the columns of $(M^h)^{-1}$ and of the magnetic and elastic constants.

3. SWIMMING WITH SINUSOIDAL FIELDS

The most commonly used actuating strategy for straight swimming in experiments is to apply the superposition of a static magnetic field to orient the swimmer in the desired direction and a perpendicular sinusoidal field to actuate the swimmer. This induces a planar symmetric beating of the tail of the swimmer, allowing a horizontal displacement. This actuation strategy will be used as a benchmark to compare with the optimal solutions. The hydrodynamical and elastic parameters of the model were fitted on experimental data (El Alaoui-Faris et al. (2020)) for the characterization of the swimmer. Using these parameters, we are able to simulate the velocity-frequency response curve of the swimmer (Fig. 3), using a magnetic field of the form :

$$\mathbf{B}(t) = (B_x, B_y \sin(2\pi ft), 0). \quad (13)$$

The velocity-frequency response curve of the swimmer shows a behaviour typical of flagellar low Reynolds swimmers, as it shows an increase of the swimming velocity until a cut-off frequency (1.5 Hz) where the velocity decreases slowly beyond this value.

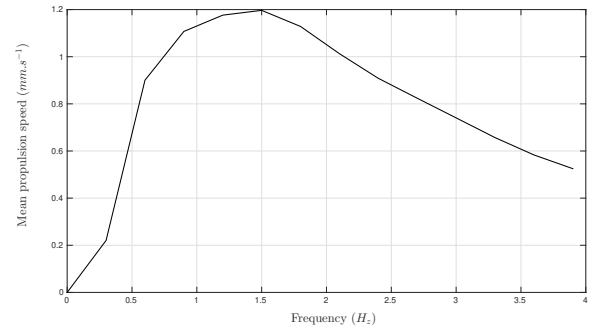


Fig. 2. Simulated velocity-frequency response curve of the swimmer.

4. OPTIMAL CONTROL PROBLEMS

The purpose of this paper is to find the time-varying magnetic field $B = \begin{pmatrix} B_x(t) \\ B_y(t) \\ B_z(t) \end{pmatrix}$ that maximizes the horizontal displacement of the swimmer at a fixed time t_f . Denoting

by $\mathbf{Z}(t)$ the state vector $\begin{pmatrix} \mathbf{X}(t) \\ \Theta(t) \\ \Phi(t) \end{pmatrix}$ and rewriting equation

(12) as $\dot{\mathbf{Z}}(t) = f(\mathbf{Z}(t), B(t))$, this optimal control problem is written as :

$$\begin{cases} \max x(t_f) \\ \dot{\mathbf{Z}}(t) = f(\mathbf{Z}(t), \mathbf{B}(t)) \\ \mathbf{Z}(0) = 0 \\ \mathbf{B}(t) \in C \end{cases}, \quad (14)$$

where C is the set of constraints on the magnetic field and t_f is the final time fixed at $3s$. We investigate four optimal control problems depending on the types of constraints on the actuating magnetic field, taking in each case the same bounds on the magnetic field intensities.

- (1) In the first optimal control problem (OCP1), we consider the admissible controls as the superposition of a static orientating field along the x axis and a time-varying field along the y axis :

$$C_1 = \{\mathbf{B}(t), B_x(t) = 2.5mT, |B_y| \leq 10mT, B_z(t) = 0\}$$

- (2) In the second optimal control problem (OCP2), both the x and y components of the magnetic field are time-varying.

$$C_2 = \{\mathbf{B}(t), B_z(t) = 0, \|(B_x(t), B_y(t))\| \leq 10mT\}$$

- (3) In the third problem (OCP3), we consider the admissible controls to be the superposition of a static orientating field along the x axis and a time-varying actuating field in the $y - z$ plane.

$$C_3 = \{\mathbf{B}(t), B_x = 10mT \|(B_z(t), B_y(t))\| \leq 10mT\}$$

- (4) In the last optimal control problem (OCP4), we consider the general case where all components of the magnetic field are time-varying.

$$C_4 = \{\mathbf{B}(t), \|(B_x(t), B_z(t), B_y(t))\| \leq 10mT\}$$

5. NUMERICAL SOLUTIONS

We use a direct method for solving the aforementioned optimal control problems. The optimal control solver ICLOCS (Falugi et al. (2010)) is used for the resolution. It discretizes the problem into a non-linear programming problem which is then solved by the interior-point solver IPOPT (Wächter and Biegler (2006)). Fig. 3 shows the displacements of the swimmer under each optimal solution, and under the sinusoidal field at the optimal frequency (1.5 Hz). We see that non-planar solutions largely out-performs planar solutions. None of the optimal solutions display singular arcs. Accordingly, and following Pontryagin's maximum principle, the solution of the single input problem OCP1 is a sequence of bang arcs and the solutions of the other problems are continuous.

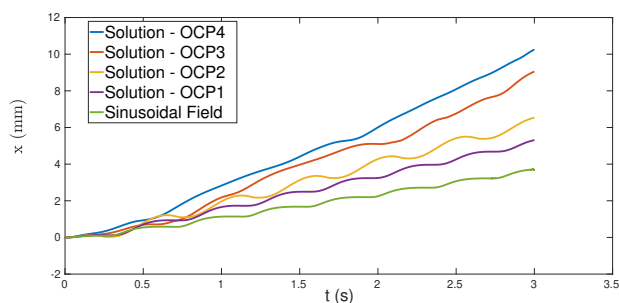


Fig. 3. Comparison of x -displacements associated with the solutions of OCP1-4 and with the sinusoidal actuation

5.1 Planar Solutions

For OCP1 and OCP2, the dimension of the dynamic system reduces to $N+3$ because of the fact that the constraints on the controls leads to a planar trajectory in the $x - y$ plane. The numerical solution for OCP1 takes the form of a sequence of Bang arcs, as seen in Fig. (4, (a)) whereas the solution of OCP2 is continuous ((b), (c)). In both cases, the optimal actuation patterns lead to a trajectory where swimmer oscillates around the x axis while moving in the x -direction (see Fig. 5).

The shape of both optimal trajectories is similar to the trajectory of the swimmer under the sinusoidal field. Interestingly enough, the optimal magnetic fields are periodic in both cases, and induce a periodic deformation of the swimmer, as seen in Fig. 6. Both solutions out-perform the reference sinusoidal actuation in terms of horizontal speed.

In practice, the solution of OCP-1 shows that having an orthogonal actuating field (in addition to the static orientating field) in the form of a square signal is more efficient than an actuating sinusoidal field. The solution of the second planar problem (OCP-2) shows that orientating fields are not necessary for straight swimming and that actuating a flagellar magnetic swimmer with two time-varying components leads to a substantial increase in swimming speed.

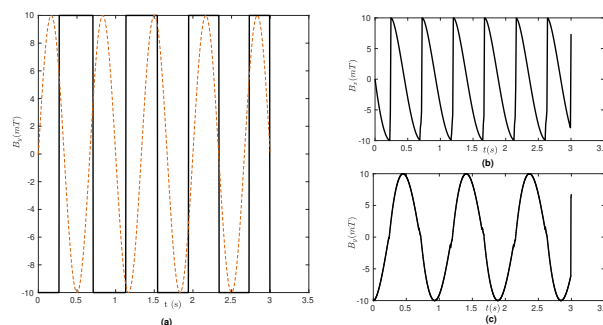


Fig. 4. Solution of the planar optimal control problems. (a) : y -component of the solution of OCP-1 compared with the sinusoidal field at optimal frequency (1.5Hz). (b) : x -component of the solution of OCP-2. (c) : y -component of the solution of OCP-3.

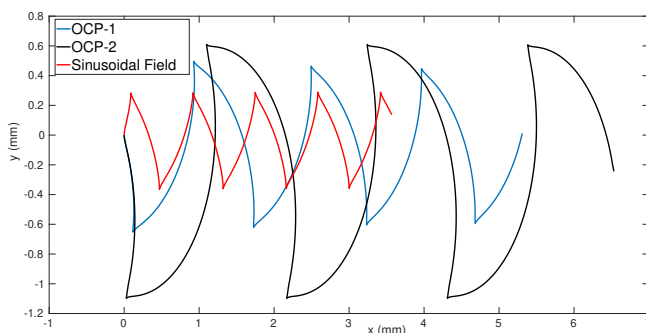


Fig. 5. Optimal planar trajectories associated with OCP-1 and OCP-2 compared with the trajectory of the swimmer actuated by the sinusoidal field.

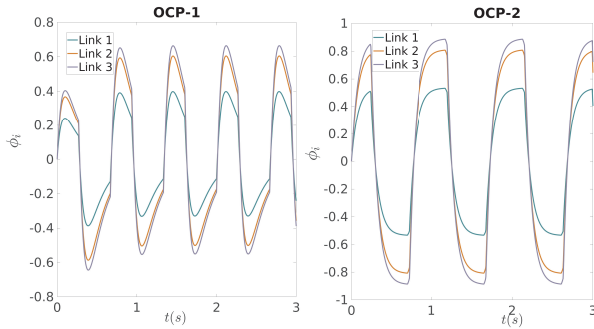


Fig. 6. Shape angles of the swimmer for the solutions of both planar problems OCP-1 and OCP-2.

5.2 Non-planar solutions

The non-planar optimal magnetic fields solutions of OCP3 and OCP4 leads to trajectories ,shown in Fig. 8, where the swimmer revolves around the horizontal axis.

As seen in Fig. 3, the non-planar actuation patterns largely out-performs the planar ones, which shows the necessity of allowing flagellar swimmers to go out-of-plane in order to swim at a maximal propulsion speed. Similarly to the planar case, the optimal solution is periodic apart from transient states near the initial and final times (see Fig. 7) and induce a periodic 3D deformation of the tail of the swimmers, as shown in the phase planes of Fig. 9.

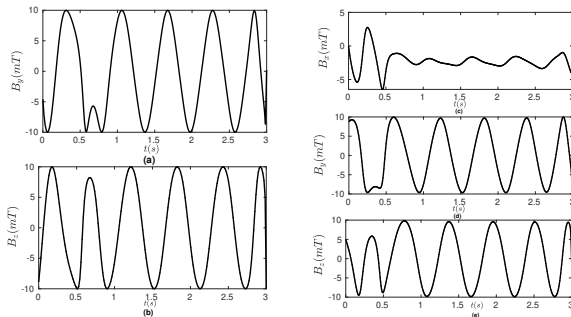


Fig. 7. Solution of the non-planar optimal control problems. (a) : y-component of the solution of OCP-3. (b): z-component of the solution of OCP-2. (c) : x-component of the solution of OCP-4. (d) : y-component of the solution of OCP-4. (e) : z-component of the solution of OCP-4.

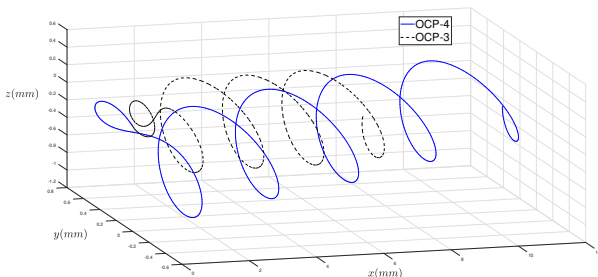


Fig. 8. Trajectories of the swimmer associated with the solutions of OCP-3 and OCP-4.

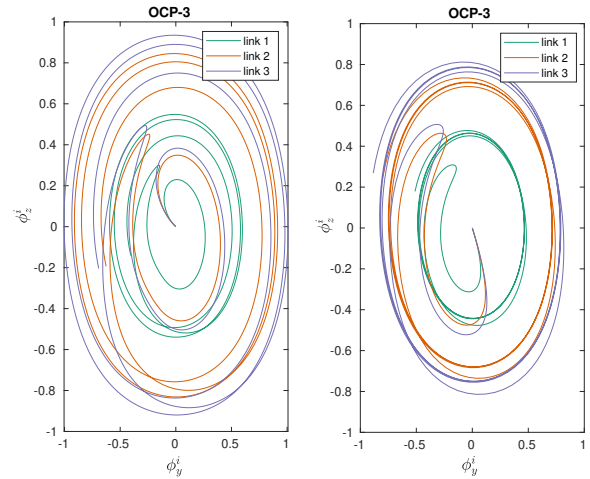


Fig. 9. Shape variables of the swimmer when actuated by the non-planar optimal magnetic fields (OCP3 and OCP4). Phase portrait of the relative angles in the $(\phi_y^i - \phi_z^i)$ for each link i of the tail.

5.3 Influence of the number of links on the trajectory and shape of the swimmer

An analysis of the influence of the number of links of the model on the optimal trajectories and magnetic fields have been made for OCP4. We define the relative trajectory error E_{tr} as :

$$E_{tr} = \frac{\|\mathbf{X}_N - \mathbf{X}_{N-1}\|_\infty}{\|\mathbf{X}_N\|_\infty}, \quad (15)$$

where \mathbf{X}_N is the optimal trajectory using N links for the tail. Similarly, we define the relative solution error E_{sol} as :

$$E_{sol} = \frac{\|\mathbf{B}_N - \mathbf{B}_{N-1}\|_\infty}{\|\mathbf{B}_N\|_\infty}, \quad (16)$$

where \mathbf{B}_N is the optimal magnetic field using N links for the tail.

Fig. 10 shows the evolution of the relative trajectory and solution errors for $N = (1 \dots 9)$. We notice that the optimal magnetic field and the optimal trajectory only marginally changes when increasing the number of links beyond 3. This shows that a 3-linked tail is enough for the optimization of the actuation of flagellar magnetic swimmers, which further emphasizes the low computational cost of our model.

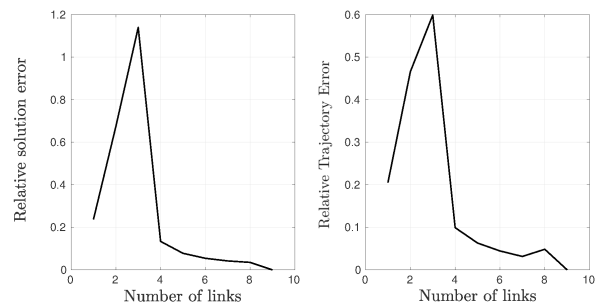


Fig. 10. Relative optimal trajectories and solution errors for an increasing number of links of the tail of the swimmer.

6. CONCLUSION AND PERSPECTIVES

In this paper, we have presented a simplified 3D dynamical model for flagellar micro-swimmers based on Resistive Force Theory and shape discretization, which circumvents the numerical drawbacks of continuum mechanics-based models. This model was used to investigate different planar and non-planar optimal actuation strategies for magnetic micro-swimmers that out-perform the commonly used sinusoidal actuation. In particular, the non-planar actuation strategies lead to a novel 3D trajectory and are significantly more efficient than the planar ones.

Another result stemming from the numerical simulations is the investigation of optimal actuation strategies that do not rely on a static orientating magnetic field, as allowing all the components of the magnetic field to be time-varying leads to an increase in swimming speed. However, these actuation methods lead to larger oscillations of the swimmer around the swimming direction, which could be an inconvenient for some experimental settings such as path following.

Beyond the present study, the simplified model presented in our model allows for easy numerical optimization studies for micro-swimmers such as parameter fitting or optimal motion planning for magnetic swimmers. It has been successfully used to optimize the displacements of an experimental swimmer in (El Alaoui-Faris et al. (2020)). It can also be easily adapted to model biological flagellar micro-swimmers. Ongoing work includes optimization of the swimming speed for more complex cost functions (maximization of efficiency, path following ..) and adapting the model for swimming in complex environments (for example in a narrow channel or in presence of a wall). Theoretical study of the optimal control problems is also a perspective of this work.

REFERENCES

- Alouges, F., DeSimone, A., Giraldi, L., and Zoppello, M. (2013). Self-propulsion of slender micro-swimmers by curvature control: N-link swimmers. *International Journal of Non-Linear Mechanics*, 56, 132–141.
- Alouges, F., DeSimone, A., Giraldi, L., and Zoppello, M. (2015). Can magnetic multilayers propel artificial microswimmers mimicking sperm cells? *Soft Robotics*, 2(3), 117–128.
- Dreyfus, R., Baudry, J., Roper, M.L., Fermigier, M., Stone, H.A., and Bibette, J. (2005). Microscopic artificial swimmers. *Nature*, 437(7060), 862.
- El Alaoui-Faris, Y., Pomet, J.B., Régnier, S., and Giraldi, L. (2020). Optimal actuation of flagellar magnetic microswimmers. *Physical Review E*, 101(4), 042604.
- Falugi, P., Kerrigan, E., and Wyk, E. (2010). Imperial college london optimal control software (iclocs). *Online: <http://www.ee.ic.ac.uk/ICLOCS>*.
- Fusco, S., Sakar, M.S., Kennedy, S., Peters, C., Bottani, R., Starsich, F., Mao, A., Sotiriou, G.A., Pané, S., Pratsinis, S.E., et al. (2014). An integrated microrobotic platform for on-demand, targeted therapeutic interventions. *Advanced Materials*, 26(6), 952–957.
- Gray, J. and Hancock, G. (1955). The propulsion of sea-urchin spermatozoa. *Journal of Experimental Biology*, 32(4), 802–814.
- Khalil, I.S., Dijkslag, H.C., Abelmann, L., and Misra, S. (2014). Magnetosperm: A microrobot that navigates using weak magnetic fields. *Applied Physics Letters*, 104(22), 223701.
- Lowe, C.P. (2003). Dynamics of filaments: modelling the dynamics of driven microfilaments. *Philosophical Transactions of the Royal Society of London B: Biological Sciences*, 358(1437), 1543–1550.
- Mack, M.J. (2001). Minimally invasive and robotic surgery. *Jama*, 285(5), 568–572.
- Moreau, C., Giraldi, L., and Gadelha, H.A.B. (2018). The asymptotic coarse-graining formulation of slender-rods, bio-filaments and flagella. *Journal of the Royal Society Interface*.
- Oulmas, A., Andreff, N., and Régnier, S. (2017). 3d closed-loop motion control of swimmer with flexible flagella at low reynolds numbers. In *Intelligent Robots and Systems (IROS), 2017 IEEE/RSJ International Conference on*, 1877–1882. IEEE.
- Patra, D., Sengupta, S., Duan, W., Zhang, H., Pavlick, R., and Sen, A. (2013). Intelligent, self-powered, drug delivery systems. *Nanoscale*, 5(4), 1273–1283.
- Qiu, F., Fujita, S., Mhanna, R., Zhang, L., Simona, B.R., and Nelson, B.J. (2015). Magnetic helical microswimmers functionalized with lipoplexes for targeted gene delivery. *Advanced Functional Materials*, 25(11), 1666–1671.
- Tornberg, A.K. and Shelley, M.J. (2004). Simulating the dynamics and interactions of flexible fibers in stokes flows. *Journal of Computational Physics*, 196(1), 8–40.
- Wächter, A. and Biegler, L.T. (2006). On the implementation of an interior-point filter line-search algorithm for large-scale nonlinear programming. *Mathematical programming*, 106(1), 25–57.
- Yates, G.T. (1986). How microorganisms move through water: the hydrodynamics of ciliary and flagellar propulsion reveal how microorganisms overcome the extreme effect of the viscosity of water. *American scientist*, 74(4), 358–365.
- Ye, Z., Régnier, S., and Sitti, M. (2014). Rotating magnetic miniature swimming robots with multiple flexible flagella. *IEEE Transactions on Robotics*, 30(1), 3–13.